Aerogel Ring Imaging Čerenkov Counter

1 Physics Requirements

Identification of charged particles over the full kinematic range is one of the basic requirements for the upgraded Belle detector. The RICH, as described in this section, has been designed to separate kaons from pions over most of their momentum spectrum in the forward (endcap) part of the spectrometer (Fig. 1), and to provide discriminaton between pions, muon and electrons below 1 GeV/c.

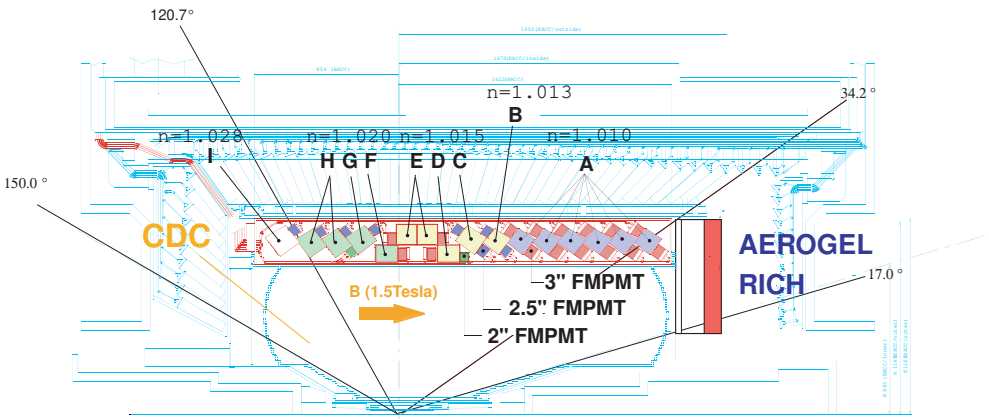

Fig. 1. *Side view of the Belle spectrometer with the proximity focusing RICH counter.*

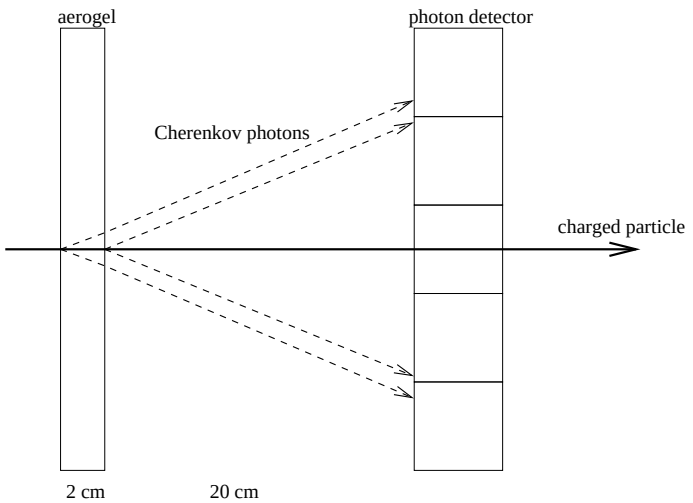

Fig. 2. *Proximity focusing RICH - principle*

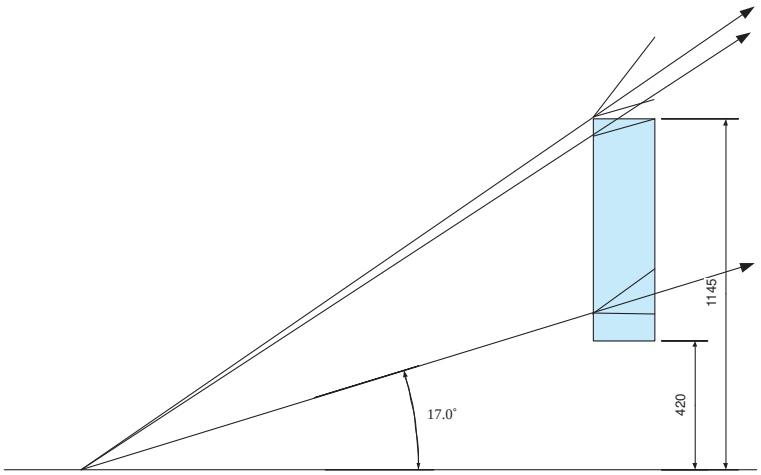

Fig. 3. *Design considerations at the edges of counter acceptance.*

2 Detector Design Considerations

The elements of the proximity focusing RICH counter are (Fig. 2):

- a *radiator* where Čerenkov photons are produced by charged particles,
- an *expansion volume* to allow Čerenkov photons to form rings on the photon detector surface,
- an array of *vacuum based position sensitive photon detectors*, that is capable of detecting single photons in a high magnetic field with high efficiency and with good resolution in two dimensions, and
- a *photon detector read-out system*.

The design choices are governed by the following criteria:

- To achieve the necessary performance, enough photons (about 10) have to be detected for each ring image at least for one of the particle species. This requirement fixes the length of the aerogel radiator to a few centimeters.
- The required resolution in the measurement of the Čerenkov angle with such a photon detector is only achievable if the expansion gap is at about 20 cm, and the radiator thickness does not exceed a few centimeters, while the photon detector granularity is at about a few milimeters.

Additional input for some details in design come from the geometrical considerations as depicted in Fig. 3. From it we deduce that at the outer edge the photon detector will only cover halfs of the rings. On the inner side, however, teh photon detector does not have to start right at the inner edge to cover full rings corresponding to tracks at the lower edge of the acceptance at 17^0.

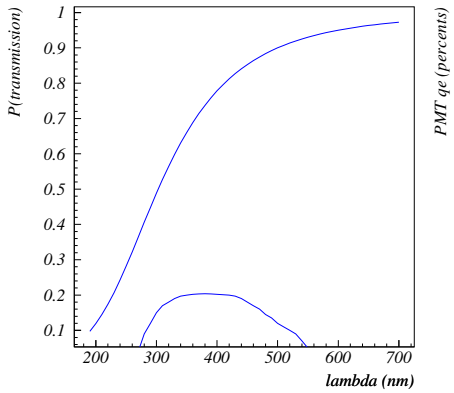

Fig. 4. *Transmission curve for the aerogel radiator (2 cm) [14] and the quantum efficiency of a typical multi-alkali PMT (H8500 [13]).*

3 Radiator

The Čerenkov radiator is aerogel, a material which is already used in the present Belle ACC (Aerogel Cherenkov Counter). A plane with 2 cm thick radiator tiles is mounted perpendicularly to the beam direction (Fig. 1). This radiator was chosen since it combines low mass and a low Čerenkov threshold. For aerogel with refractive index $n = 1.05$ the Čerenkov threshold momenta for pions is at 0.63 GeV/c, and the Čerenkov angle corresponding to $\beta = 1$ particles amounts to $\theta_c = 310$ mrad. In Table 1 the properties of the radiators with two refractive indices, 1.05 and 1.03, are listed for comparison. of the two radiators, the one with $n = 1.05$ was chosen because it has a lower threshold for Čerenkov radiation.

Table 1
Properties of aerogel radiators

refr. index	1.03	1.05
pion threshold	0.81 GeV/c	0.63 GeV/c
kaon threshold	2.83 GeV/c	2.2 GeV/c
proton threshold	5.4 GeV/c	4.2 GeV/c
maximum Čerenkov angle	242 mrad	310 mrad
$\theta_c(\pi) - \theta_c(K)$ at 4 GeV/c	31 mrad	23 mrad
$\theta_c(e) - \theta_c(\pi)$ at 0.8 GeV/c	mrad	mrad
transmission length at 400 nm	40 mm	30 mm

In Fig. 4 the transmission curve is shown for a typical 2 cm thick radiator sample. Since the losses of photons are dominated by Rayleigh scattering with a strong wavelength dependence (λ^{-4}) of the attenuation length Λ, the transmis-

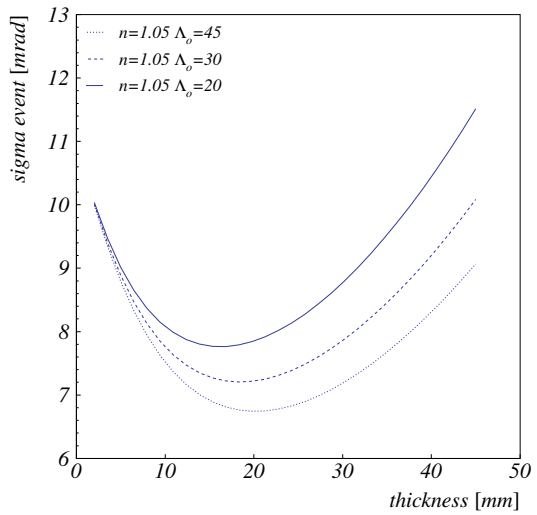

Fig. 5. *Čerenkov angle resolution per track* $\sigma_\theta^{\rm track}$ *as a function of the radiator thickness for three different attenuation lengths.*

sion varies considerably. The transmission was calculated from the measured variation of attenuation length Λ with wavelength, by integrating over the radiator depth z along the track direction

$$T(\lambda) = \int \exp\left(-\frac{z}{\Lambda(\lambda)\cos\theta_c}\right) dz. \tag{1}$$

The optimal radiator thickness was determined by ploting in Fig. 5 the figure of merit, resolution in Cherenkov angle measurement per track,

$$\sigma_\theta^{\rm track} = \frac{\sigma_\theta}{\sqrt{N_{pe}}},$$

which depends both on the resolution in Cherenkov angle measurement by a single photon σ_θ and on the number of detected photons N_{pe} (c.f. the R&D subsection, Figs. 17 and 19). The position of the minimum depends slightly on the transmission length. For a typical value of $\Lambda(400\ \text{nm}) = 30$ mm, the best performance is achieved if the radiator thickness is around 20 mm.

Two possible tiling schemes of the aerogel radiator are shown in Fig. 6. One of the advantages of the hexagonal scheme is that the fraction of surface where the photon yield gets reduced due to tile edge effects is smaller (see Fig. 21). The hexagonal tiling needs three different tiles (full hexagon with 125 mm sides and two half hexagons). The tiling with distorted squares again needs three different tiles (one for each annulus), with a maximal side of about 220 mm.

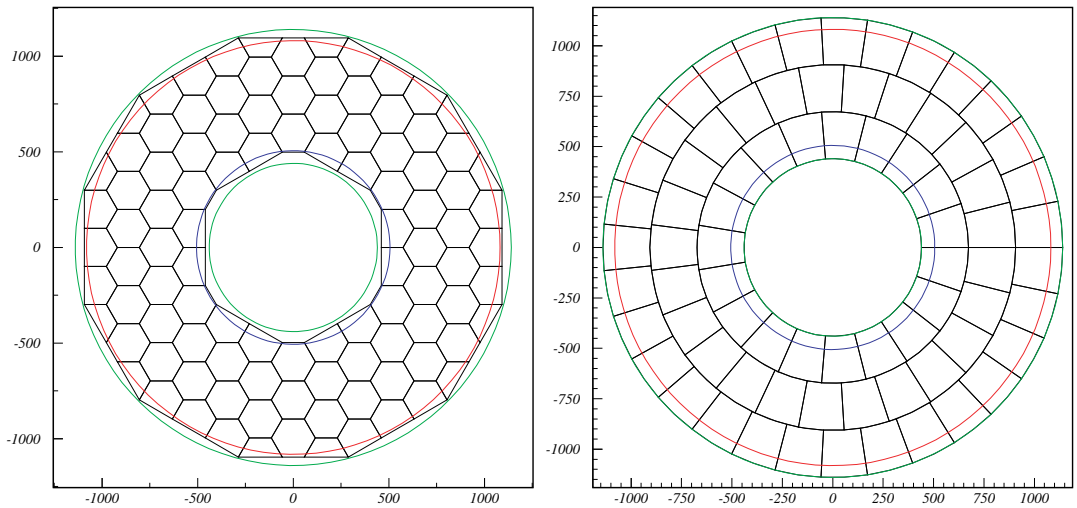

Fig. 6. *Two aerogel radiator tiling schemes. The region with incomplete rings at the outer edge is indicated by a red? circle.*

4 Photon Detector

The position sensitive photon detector covers a surface of rougly 3.5 m^2, and is an essential component of the counter. The requirements for the photon detector are summarized as follows:

- Should be immune to the 1.5 T magnetic field,
- Should have single-photon sensitivity with a good single photon peak-to-valley ratio and high detection efficiency,
- Should have position resolution (RMS) of less than 2 mm,
- Should have high sensitivity for photons of $\lambda \approx 400$ nm (c.f. Fig. 4).

There are several candidates for such a photon detector. For instance, a Micro-Channel-Plate PMT (MCP-PMT) has excellent timing properties and single-photon resolution in high magnetic field, but the collection efficiency for photo-electrons is at most 65%. A fine-mesh PMT can be operated in a high magnetic field, but has very poor single-photon resolution, such that it is hard to observe the single-photon peak. Currently we consider a proximity-focusing-type Hybrid Photo-Diode (HPD) or a Hybrid-Avalanche-Photo-Diode (HAPD) as the best candidate, since they have both excellent single-photon resolution and a high detection efficiency even in a high magnetic field. The principle of operation of an HPD can be seen in Fig. 7. Some kinds of HPD's are already commercially available [10]. However, we can not use the focusing type of HPD in a high magnetic filed, and the effective area of the currently available proximity focusing type HPD is less than 50%. In order to enlarge the detection area of an HPD, we decided to develop with Hamamatsu Photonics K.K. (HPK) a new HPD of a proximity focusing type with a pixel size of 5 mm square. Fig. 8 shows a schematic drawing of the H(A)PD, which has a

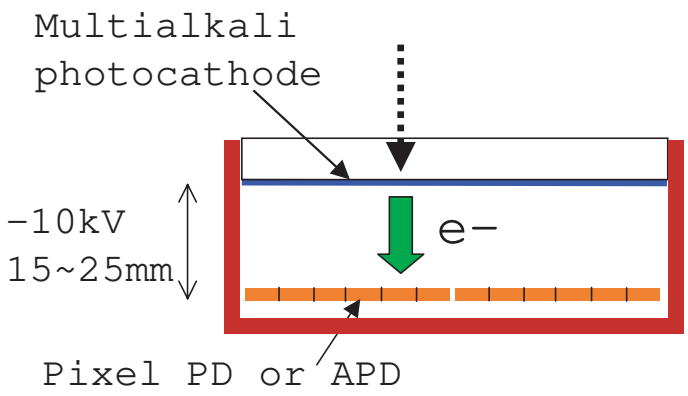

Fig. 7. *Principle of operation of a proximity focusing hybrid photon detector (HPD).*

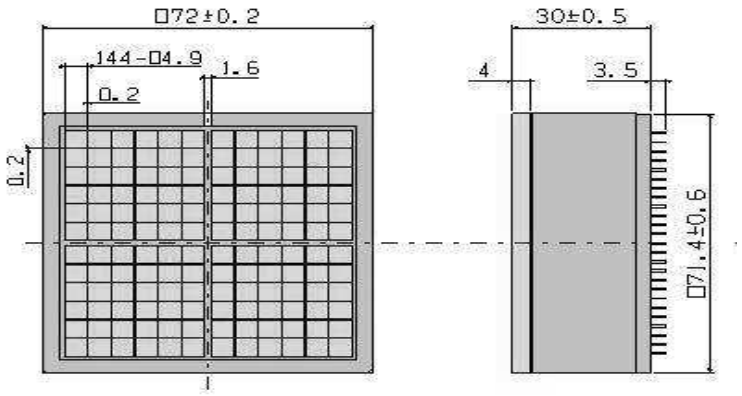

Fig. 8. *Schematics of the proximity focusing hybrid photon detector (HPD) under development.*

housing of 72x72 mm^2 and 59x59 mm^2 sensitive area. This means 67% of the total area is covered by photo-diodes (PD) or avalanche PDs (APD). Four PD's or APD's, each with a 6x6 pixel array, are installed in a ceramic vessel as shown in Fig. 8, which leads to 12x12 pixels in total. The window is made of quartz and the photocathode material is multi-alkali.

A possible tiling scheme of the photon detector surface is shown in Fig. 9. The detector surface is covered with 600 HPD PMTs, with a 92% coverage. The minimal distance between the tubes is 0.5 mm. The maximal distance is a few mm (depends on the layer), allowing a feed through for the HV cable for the photocathode at the front side of the tube.

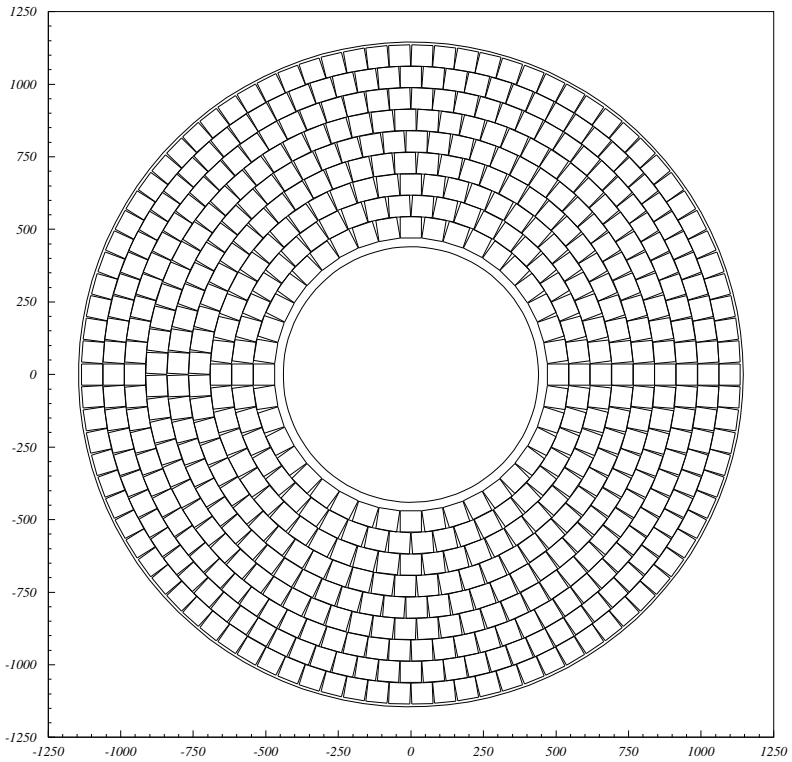

Fig. 9. *Photon detector tiling scheme.*

5 Read-Out System

In parallel to the development of the photon detector, we are developing the readout electronics. Since the number of readout channels amounts to more than 80k in total, we need a special read-out scheme to treat them. We have therefore developed an ASIC which has the following properties:

a) High gain with short shaping times, 5V/pC and 150 ns,
b) Variable gain amp to adjust the threshold, x 1-16,
c) Pipeline readout scheme with shift register,
d) Low power consumption, 5 mW/ch.

A schematic of the ASIC and a photo through microscope are shown in Fig. 10. Only the on/off information after the comparator are registered in the shift register. When a trigger signal is accepted, the last 4 bits of the shift register are duplicated in a 4-bits register, which is read out serially.

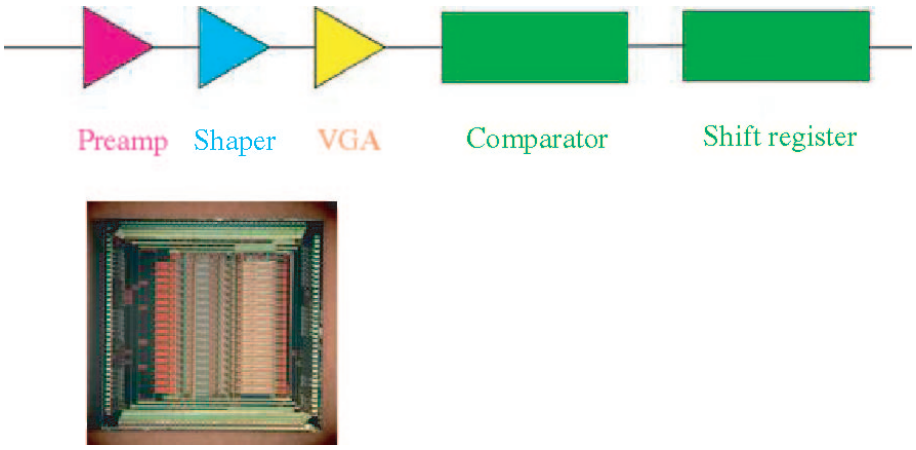

Fig. 10. *Schematic and photo of the ASIC (4.9x4.9 mm^2).*

As a fall-back solution we could employ a low noise read-out system based on the type used in the Belle silicon vertex detector (SVD), but adapted to the special needs of a single photon detector with pads. The system, an upgrade of the integrated circuit used in the CleoIII RICH [19], employs two chips, VA64tap with preamplifiers, amplifiers and discriminators for 64 channels, and LS64 with a 64 channel logic level adaptor stage [20]. The full read-out chain of the chip could be designed in a very similar way as for the read-out for the SVD2 counter.

6 Expected performance

6.1 Number of photons

The expected number of Čerenkov photons is shown in Table 2. Both values have been calculated by combining the measured values for quantum efficiency $\epsilon_q(\lambda)$ [13] and aerogel transmission $T(\lambda)$ (Fig. 4). The number of photons was calculated by using the relation

$$N_{phot} = 370\mathrm{cm}^{-1}\; d\; \epsilon_e\; \epsilon_a\; \sin^2\theta_c \int \epsilon_q(\lambda)\; T(\lambda)\; \lambda^{-2}\; d\lambda, \qquad (2)$$

where d is the radiator thickness (2 cm), ϵ_e is the single photo-electron pulse detection efficiency, and ϵ_a is the active surface fraction of the photon detector surface (Table 2).

Table 2
Efficiencies and number of photons. ϵ_e is the single electron pulse detection efficiency, ϵ_a the fraction of active surface of a single module, and ϵ_t the fraction of the surface covered with photon detector modules in a particular tiling scheme (Fig. 9). For quantum efficiency and aerogel transmission see Fig. 4.

photon detector	HPD	MCP-PMT
ϵ_a	0.67	0.66
ϵ_e	0.70	0.60
ϵ_t	0.92	0.92?
number of photons	10?	10?

6.2 Resolution of the RICH

From the photon hit coordinate as measured by the photon detector and from the particle trajectory as given by the tracking chamber, the photon direction is reconstructed to obtain the Čerenkov angle and thus the velocity βc of the particle. Sources of error in the measurement with a single photon are:

- The finite coordinate resolution of the photon detector

$$\sigma_\theta^{pix} = \frac{a}{\ell\sqrt{12}} \cos^2\theta_c = 6.4 \text{ mrad}, \tag{3}$$

  with a pad size of $a = 4.9$ mm and the radiator to photon detector distance of $\ell = 20$ cm.
- The finite radiator thickness $d = 2$ cm

$$\sigma_\theta^{emp} = \frac{d}{\ell\sqrt{12}} \sin\theta_c \cos\theta_c = 8.4 \text{ mrad}, \tag{4}$$

- The chromatic error, a consequence of dispersion, the variation of the refractive index over the energy range of those Čerenkov photons that are detected by the photon detector. From the measured variation of refractive index with wavelength, the transmission of aerogel and the photo-detector quantum efficiency (Fig. 4), the R.M.S. spread σ_n in refractive index can be determined, from which

$$\sigma_\theta^{dis} = \frac{\sigma_n}{n} \frac{1}{\tan\theta_c} = 2 \text{ mrad}. \tag{5}$$

- The error due to the imperfections and inhomogenuity of the radiator. From the experience with the HERMES RICH [7] we conclude that the resulting contribution amounts to

$$\sigma_\theta^{rin} = 2 \text{ mrad}. \tag{6}$$

- The error arising from the error in track parameters as determined by the tracking system and extrapolated to the radiator. The error in the track direction can be parametrized as

$$\sigma_{dir} = 1.4 \text{ mrad}\sqrt{1 + (1.4\text{GeV}/p)^2} \tag{7}$$

while the error in track position on the radiator entry plane is

$$\sigma_{pos} = 0.2 \text{ mm}\sqrt{1 + (1.75\text{GeV}/p)^2}. \tag{8}$$

The resulting error in Čerenkov angle amounts to:

$$\sigma_\theta^{tr} = 10 \text{ mrad}\sqrt{1 + (1.75\text{GeV}/p)^2}. \tag{9}$$

The combined single photon error is finally obtained by summing the above errors in squares. For 4 GeV/c momentum tracks it amounts to

$$\sigma_\theta = 14 \text{ mrad} \tag{10}$$

Assuming 10 detected photons for a $\beta = 1$ particle, the measurement precision is

$$\sigma_\theta^{(N)} = \frac{\sigma_\theta}{\sqrt{N}} = 4.5 \text{ mrad}. \tag{11}$$

In absence of backgrounds, the proposed counter would thus enable a 5σ pion-kaon separation at the kinematic limit of 4 GeV/c. Pions would be separated at a 4σ level from electrons up to about 1 GeV/c.

6.3 Background

Since the number of photons per ring is rather low, backgrounds could degrade the performance as discussed above. The following sources of background expected in the RICH photon detector were considered:

1. Rayleigh scattered Čerenkov photons from the same track.
2. Čerenkov photons emitted by the same track in the photon detector window.
3. Čerenkov photons emitted by other charged tracks in the event.
4. Čerenkov photons emitted by products of primary photon conversion in the material in front of the RICH radiator and in the radiator itself.
5. Beam related background hits.
6. Electronic noise.

Table 3
Thickness of materials in the RICH in units of radiation length X_0.

Layer	Thickness mm	Thickness X_0
Radiator		
aerogel	20	0.001
support structure	?	?
Photon detector		
PMT window	4 mm	0.03
PMT body	?	?
read-out electronics	?	?

The levels of backgrounds (1) and (2) were estimated from the test beam data (c.f. the R&D subsection, Fig. 16a), and turned out to be the dominant source.

The levels of backgrounds (3) and (4) were studied by computer simulation. Because of a rather small diameter of Čerenkov rings (12 cm) as compared to the typicall distance between track impact points on the aerogel radiator, the background (3) does not contribute significantly. This is also illustrated by a typicall event displayed in Fig. 11.

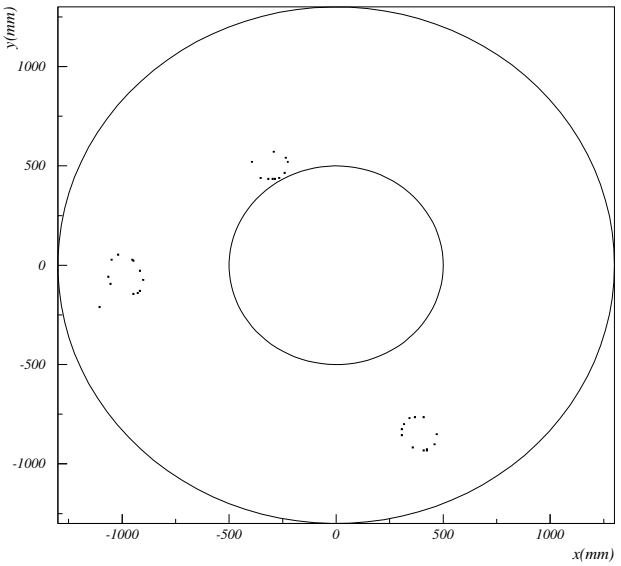

Fig. 11. *A typical MC generated event as seen by the aerogel RICH.*

The level of source (5) was estimated from the current background rate in the endcap ACC, and scaled by a factor of 20 as expected from the luminosity increase. This rough estimate yields values from 60 Hz/cm^2 to 140 Hz/cm^2 for

the modules at the maximum and minimum radial distance from the beam. Finally, the electronic noise is estimated by assuming a conservative value of 10^{-3} for the probability of a noise hit.

In total, we expect 0.7 smoothly distributed background hits within the annulus of $\pm 3\sigma_\theta$ of the 4 GeV/c pion ring.

Table 4
Estimated number of background hits within the annulus $\pm 3\sigma_\theta$ of the 4 GeV/c pion ring.

Type of background	hits/ring
Scattered photons	0.5
Beam related background	0.002
Electronic noise	0.2
Total	0.7

6.4 Particle identification capabilities

The particle identification capabilities of the counter were evaluated by using simulated data. The backgrounds which are not included in simulation (sources 1,2,5,6) were generated according to observed or expected rates.

7 R&D Results

Aerogel radiator

The hydrophobic aerogel with a low refractive index ($n = 1.01 \sim 1.03$), as developed for the Belle-ACC, is characterized by a high transmission length ($\sim$ 40 mm at a wave length of 400 nm). However, the transmission length of aerogel with a higher refractive index of $n = 1.05$ fell below one half the value if compared to the aerogel with $n = 1.03$. Keeping in mind that for a collider experiment a hydrophobic aerogel is preferred to a hydrophilic one, we reexamined the hydrophobic aerogel production technique in a joint development with Matsushita Electric Works Ltd.

As a result, we found that the important factors determining the transmission length are the solvent and selection of the precursor to be used for its production. Originally, we used methyl-alcohol for the solvent, and methyl-silicate as a precursor [5]. When we applied di-methyl-formamide (DMF) [16], and changed the supplier of the precursor, we could improve the transmission

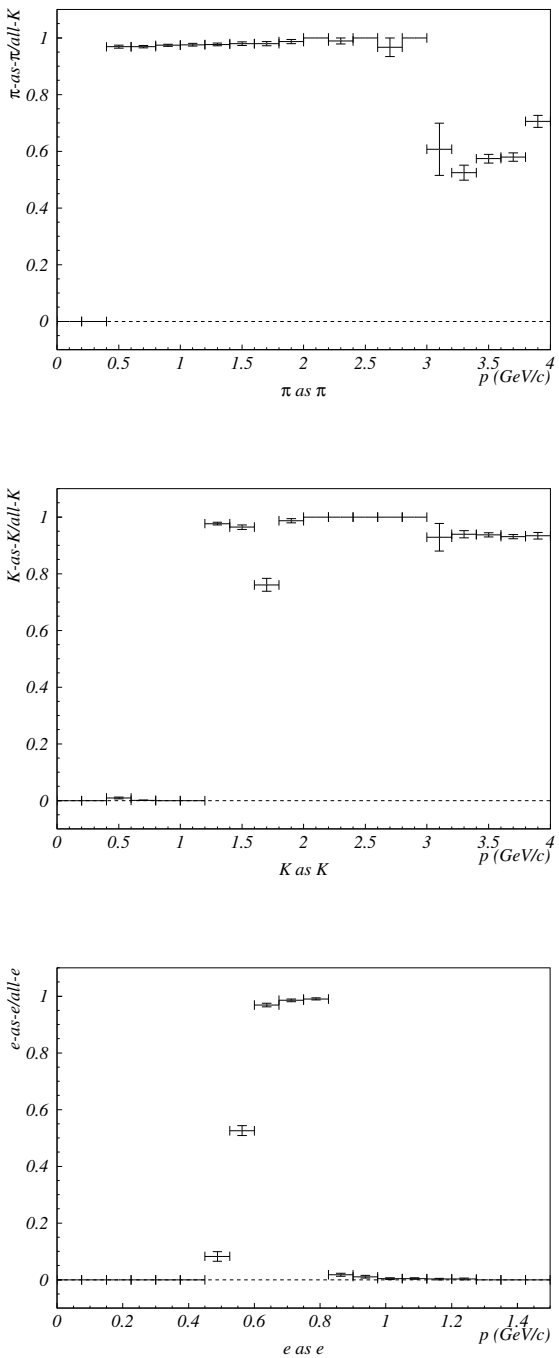

Fig. 12. *Particle identification capabilities of the aerogel RICH counter (from top to bottom): pion identification efficiencies at 5% kaon misidentification probability, kaon and electron efficiencies at 5% pion misidentification probability.*

length of the aerogel. Fig. 13 shows the refractive indices of aerogel and the

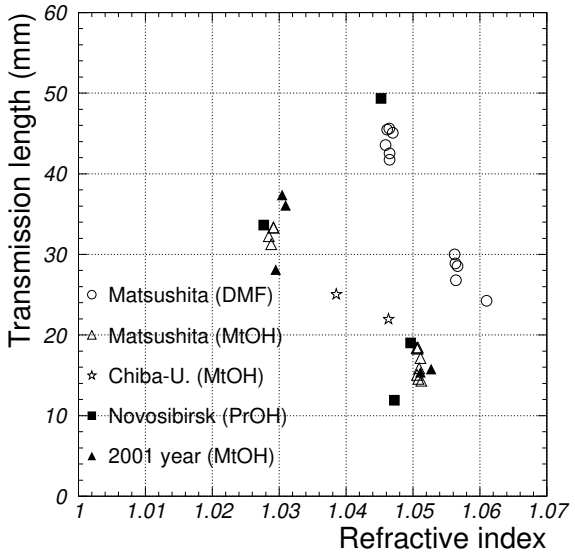

Fig. 13. *Transmission length at 400 nm and refractive index at 405 nm for the aerogel samples used in the test.*

relation to transmission length for samples which were used in this beam test. The refractive index was determined by measuring the deflection angle of laser light (laser diode: 405 nm) at a corner of each aerogel tile; the transmission length was measured with a photo-spectrometer (Hitachi U-3210). In addition to the samples produced with the new technique at Matsushita Electric Works Ltd. and Chiba University, samples from BINP (Novosibirsk) were tested [17]; for comparison, we also tested the samples used in the previous beam test. The Matsushita(DMF) samples are clearly superior to other hydrophobic aerogels.

System test

In a series of beam tests we have checked the performance of a complete system. While in the first test [11] at the KEK-PS $\pi 2$ beam line an array of multi-anode PMTs (Hamamatsu R5900-M16) was used for photo-detection, the recently developed flat-panel PMTs, Hamamatsu H8500, were employed in the second one [12]. 16 PMTs were used in a 4×4 array and aligned with a 52.5 mm pitch, with an effective area of photon detection of 84%. At the back of each PMT, an analog memory board is attached to read out multi-channel PMT signals. Among the 16 PMTs, 8 PMTs were delivered in January, 2002, and the remaining PMTs were delivered in October, 2002. Since the manufacture method of the PMT was still under development, they exhibit a large variation in quantum efficiency and gain. The quantum efficiency at 400 nm varies between 16% and 25%; the gain varies from $1 \cdot 10^6$ to $6 \cdot 10^6$ when the maximal allowed high voltage of -1100 V is applied to the photo-cathode [15]. The PMTs from the later batch show a slightly better performance.

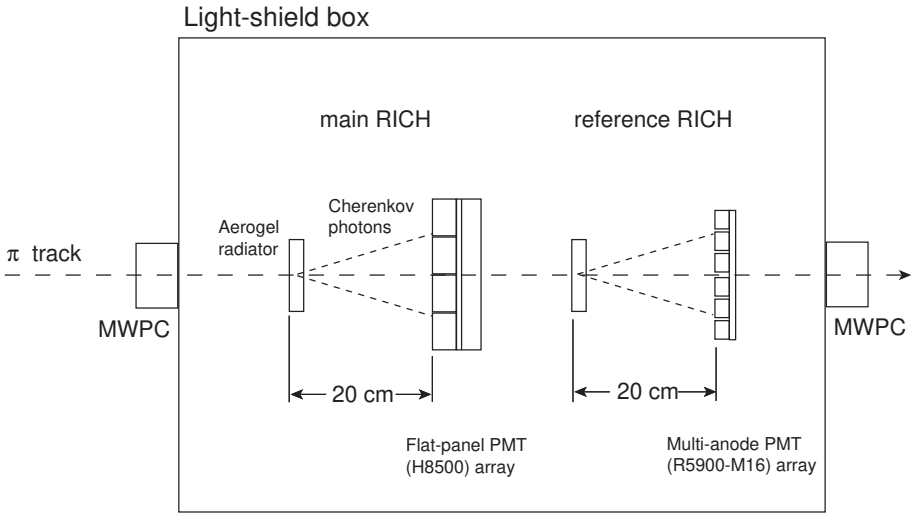

Fig. 14. *Beam test set-up.*

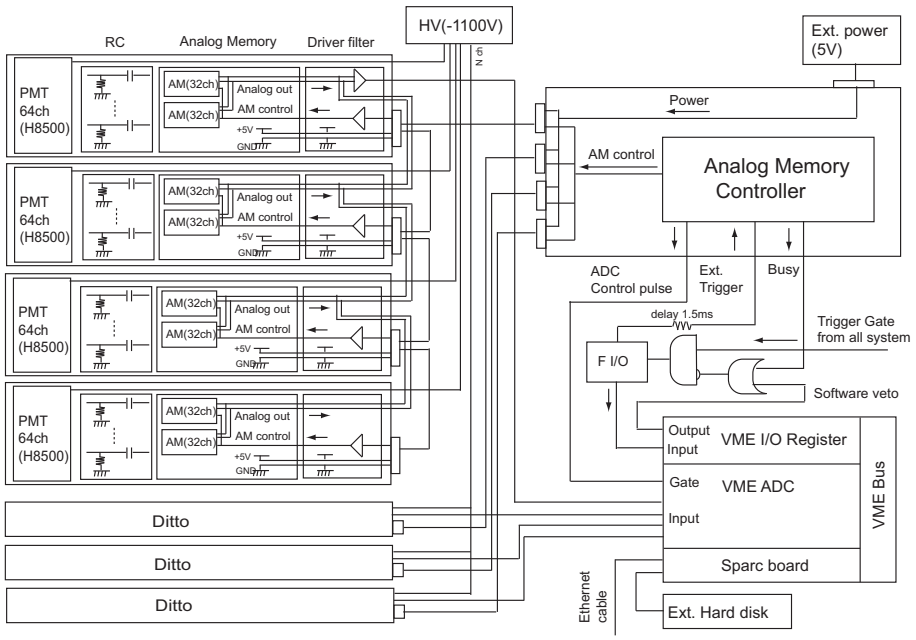

Fig. 15. *Schematics of the read-out system for the flat-panel PMTs.*

For the beam test, pions with momenta between 0.5 GeV/c and 4 GeV/c were used. Beside the RICH detector under study, counters for triggering, tracking and particle identification were employed. The set up of the aerogel RICH is shown in Figure 14. Two RICH counters were placed in a light-shield box and tested simultaneously. Each RICH was composed of a layer of aerogel radiator and a photo-detection plane, parallel to the radiator face at a distance of 20 cm. The upstream Cherenkov counter was the detector under study; the downstream counter was the one employed in the previous beam test [11]. Since the latter uses a well-known photo-detector, multi-anode PMTs Hamamatsu R5900, we regarded it as a reference. The particle trajectories were measured with multi-wire proportional chambers (MWPC) at the upstream

and downstream ends of the light-shield box.

For the beam test, a new read-out system was designed by using analog memory chips. The analog memory chip is based on a chip developed by H. Ikeda [18] for a cosmic-ray experiment. We borrowed the chips from NASDA (National Space Development Agency of Japan), and developed the chip control system. In the analog memory chip, the signals of 32 channels are preamplified, sampled in 1 μs intervals, and stored in an 8 steps deep analog pipeline. Figure 15 shows a schematic view of the readout system with these analog memories. Two 32 channel analog memories are attached to each 64 channel PMT. The memories corresponding to four PMTs are controlled by a 256 channel memory controller. When the gate pulse is formed from the trigger signal, a control signal is sent from the controller to the analog memories. The difference in the value of the analog memory between the latest and the first memory content is fed to the output. The obtained output values of 256 channels are clocked into one signal train with a period of 10 μs per channel. Each analog memory controller outputs the serial signal together with synchronized control signals. These signals are then read by a 12-bit VME ADC (DSP8112, MTT Co.) with a conversion time of 5 μs.

Most of the test measurements were performed with a π^- beam at 3 GeV/c. To systematically evaluate the detector performance, data were taken with different aerogel samples with various transmission lengths and thicknesses. Data were also taken by varying the π^- momentum in the range from 0.5 GeV/c to 4.0 GeV/c.

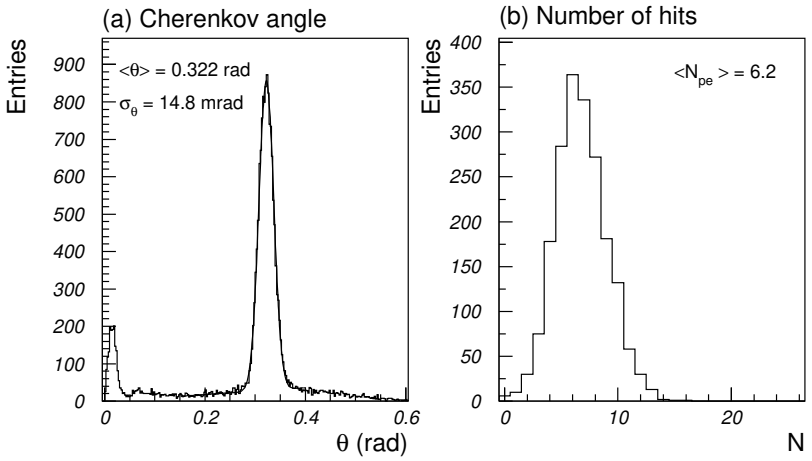

Fig. 16. *Distribution over the Cherenkov angle for single photons (a), and the number of detected photons per ring (b), for a* 20 *mm thick aerogel radiator sample with* $n = 1.056$ *and a transmission length of* 30 *mm.*

Figure 16a shows a typical distribution of the Cherenkov-angle for single pho-

tons. Cherenkov photons from the aerogel radiator are clearly seen with a low background level. The flat background hit distribution on the photon detector is consistent with the assumption that it originates from Cherenkov photons which were Rayleigh scattered in the radiator. The peak at small Cherenkov angles is due to Cherenkov radiation generated by the beam particle in the PMT window.

Cherenkov-angle resolution for single photons

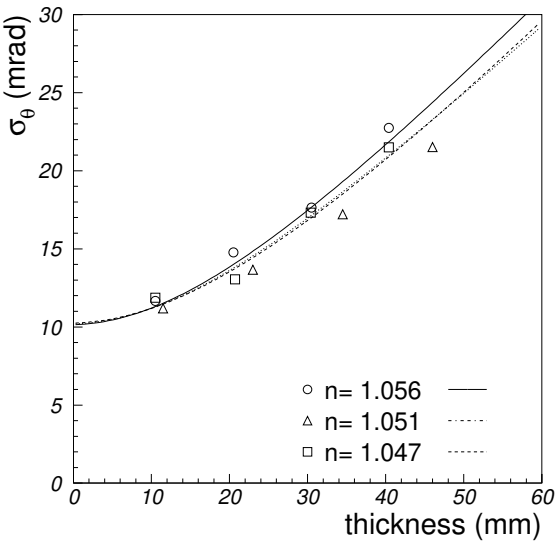

Fig. 17. *Angular resolution as a function of the aerogel thickness. The symbols correspond to the data for the different samples, and the curves correspond to the expected functions described in the text.*

The angular resolution was obtained from a fit of the Cherenkov angle distribution (Fig.16a) with a Gaussian signal and a linear function for the background. The resolution was typically around 14 mrad, independent of the refractive index. The main contributions to the resolution of the Cherenkov angle come from the uncertainty in the emission point and from the pixel size of the PMT (Eqs. 3 and 4). The measured variation of the resolution with the thickness of aerogel is shown in Figure 17 together with the expectations. The measured resolution matches the expected values reasonably well, appart from a discrepancy between the two, which could be accounted for by a constant additional contribution of about 6 mrad. The discrepancy could arise from the effect of aerogel (non-flat aerogel surface and possible non-uniformities in the refractive index due to position variation and chromatic dispersion), which are subject to further investigation. The uncertainty in the track direction is expected to be negligible at 3 GeV/c, but increases considerably at low momenta (0.5 GeV/c) due to the effect of multiple-scattering, as can be seen in Figure 18.

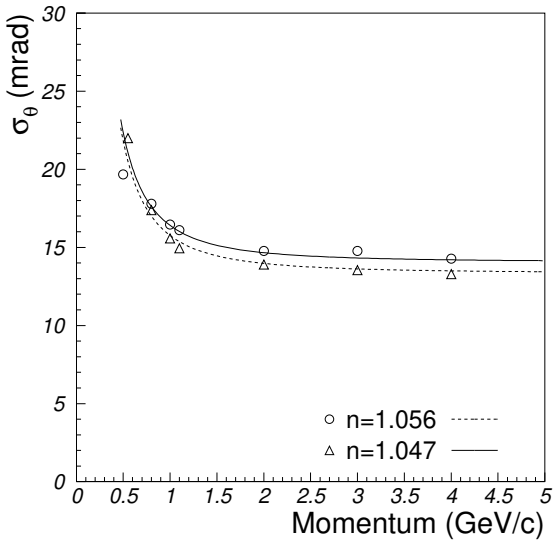

Fig. 18. *Angular resolution as a function of the charged particle momentum for two different samples. The symbols correspond to the data and the curves are fits including the effect of multiple-scattering.*

Photoelectron yield

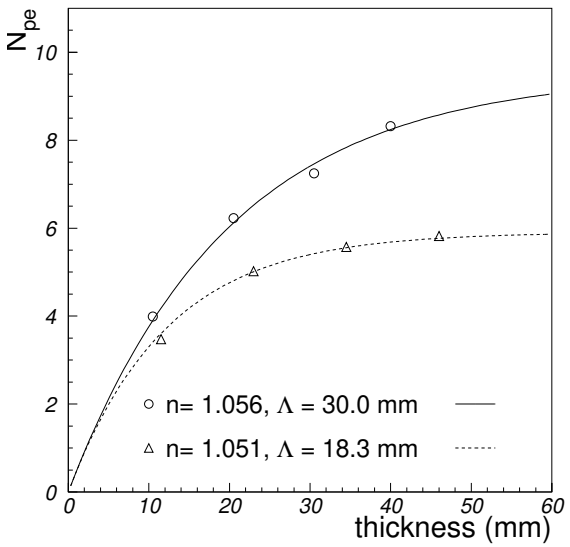

Fig. 19. *Number of detected photons per Cherenkov ring as a function of the aerogel thickness. The symbols correspond to the data and the curves are fits described in the text.*

Figure 16b shows a typical distribution of the number of hits within $\pm 3\sigma$ from the average Cherenkov angle. The number of hits for the signal region was estimated by subtracting the background from the fits to the Cherenkov-angle distribution. Figure 19 shows the dependence of the number of detected

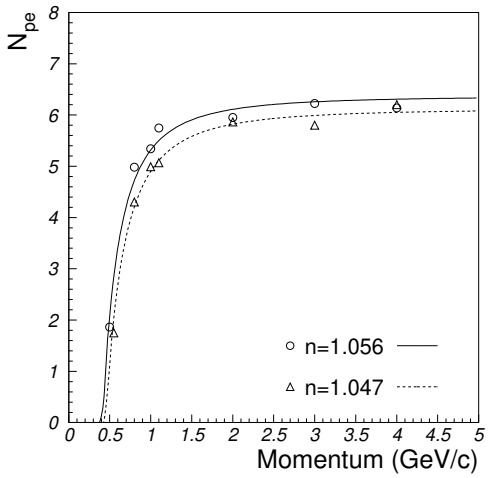

Fig. 20. *Number of detected photons per Cherenkov ring as a function of the charged particle momentum. The symbols correspond to the data, and the curves are fits described in the text.*

photons on the aerogel thickness. As expected from the expression Eq. 2, the number of photons does not linearly increase with the aerogel thickness, but saturates due to the scattering effect in aerogel. The dependence on the pion momentum, displayed in Figure 20, is fitted with the form expected from the Cherenkov relations, and shows a good agreement. For pions with momenta above 1 GeV/c, the number of detected Cherenkov photons was typically around 6 for aerogel samples with $n = 1.05$.

The performance of the RICH counter under study was compared in the same set-up with the performance of the reference counter with a well-known photon detector, Hamamatsu R5900-M16 multi-anode PMTs. Since the two counters have a different active area fraction (84% for the flat-panel PMTs, and 36% for the R5900-M16 PMTs) and a different acceptance, the comparison of the photon yields was made by normalizing to the full active surface. While the flat-panel yield for a particular case was 6.2, which resulted in 7.8 if extrapolated to the full active area, the corresponding number for the R5900-M16 was 12. It appears that this difference is mainly due to the rather low quantum efficiency and amplification of some of the flat-panel tubes employed. This, in turn, causes inefficiencies in single photon detection with a given threshold. If the best tube in the set is normalized to the full acceptance, the corresponding number increases to 10, and we would expect about 8 photons per ring.

It has been already noted by the HERMES group [7] that a loss of Cherenkov photons occurs at the side wall boundaries between adjacent aerogel tiles. We have confirmed this finding by measuring the number of photons per Cherenkov ring as a function of the distance of the charged particle impact point from the boundary between two tiles. The measurement is shown in

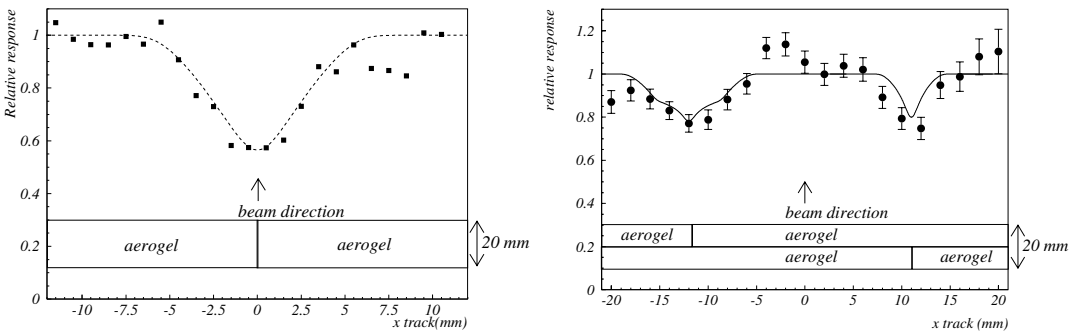

Fig. 21. *The number of Cherenkov photons detected on the ring, as a function of the charged particle impact point position on the aerogel tile. The values shown are normalized to the measured values in case of a single tile covering the full range. Also shown is the estimate of a simple model.*

Fig. 21, where a dip is seen at the tile boundaries for two different tiling schemes. In order to eliminate other geometrical factors, like for example the acceptance of the photon detector, the measured yield was normalized to the yield obtained with one tile covering the entire range. The result clearly indicates a reduction of yield when the charged particle is closer than about 5 mm to the boundary of a 2 cm thick aerogel tile. It is worth noting that a simple model, where all photons hitting the boundary between the two tiles get lost, accounts for most of the observed dependence. From the result it is clear that the tile size should be as large as possible to reduce the impact of the loss. The performance of the double shifted layer configuration shown in the right side of Fig. 21 is under study.

Particle Identification

Finally, we estimate the performance of pion/kaon separation in the momentum range of around 4 GeV/c, which is of considerable importance for the Belle experiment. If we take into account a typical measured value for the single-photon angular resolution, $\sigma_c \sim 14$ mrad, and the number of detected photons $N_{pe} \sim 6$, typical for 20 mm thick aerogel samples with $n = 1.05$, we can estimate the Cherenkov angle resolution per track to be $\sigma_c/\sqrt{N_{pe}} = 5.7$ mrad. This naive estimate is also confirmed by the direct measurement shown in Figure 22. Here, the track-by-track Cherenkov angle is calculated by taking the average of the angles measured for hits around the predicted position of the Cherenkov ring. From this we can deduce that at 4 GeV/c, where the difference of Cherenkov angles for pions and kaons is 23 mrad, a 4σ separation between the two is possible. As an additional cross check, we have also collected data with the pion beam of 1.1 GeV/c, which can be used to represent a kaon beam of 4 GeV/c (apart from a slightly larger sigma due to multiple scattering). As can be seen from Figure 22, the two peaks are well separated. Thus, the proximity focusing aerogel RICH seems to be promising for the upgrade of the Belle PID system in the forward region.

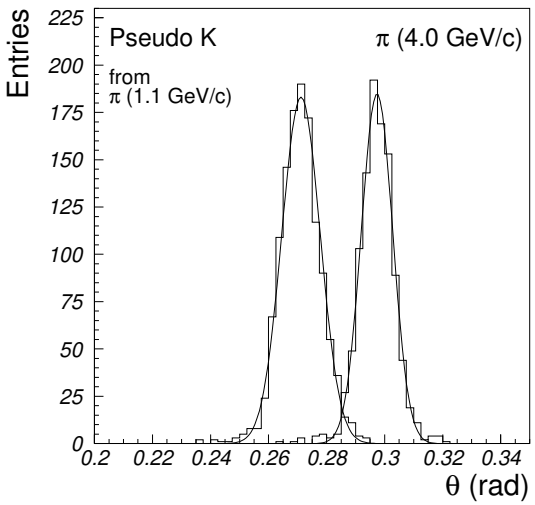

Fig. 22. *Cherenkov angle per track for pions of* 4.0 GeV/c *and* 1.1 GeV/c. *Pions at* 1.1 GeV/c *are used to represent the kaon beam of* 4 GeV/c. *The angular resolutions for* 4.0 GeV/c *and* 1.1 GeV/c *are* 5.4 *mrad and* 6.7 *mrad, and the two peaks are separated by* 4.2σ.

HPD development

Although the system test was very successful, there are still several issues which have to be solved for implementation in the Belle spectrometer. The most important item is the development of a PMT which can be operated in a high magnetic field (1.5 T). In order to confirm the ability of candidate photon detectors HPD and HAPD to efficiently detect single photons over a large active area, a single channel HPD and a 3x3 multi-channel HAPD were tested by using a laser diode light pulser ($\lambda = 850$ nm). Fig. 23 shows a multi-photon spectrum obtained by a HPD, which was operated at 8 kV for electron bombardment (EB) (typical EB gain was 1500) and 80 V for bias. The leak current was 4 nA and the detector capacitance was 20 pF.

Multi-photon spectrum was obtained also by the HAPD prototype (Fig. 24). The gain was higher ($2.6 \cdot 10^4$) in the case of the HAPD due to the avalanche gain of about 15. However, the detector capacitance was 73 pF and the leak current amounted to 14 nA, resulting in a worse signal to noise ratio than in the case of the HPD. Although both the HPD and the HAPD have shown an excellent performance, the HPD gives a slightly better resolution.

Prototype production of APD's and PD's is going on in HPK, and evaluation of the samples is being carried out. While so far there are no serious problems for the PD's except for a slightly worse timing response, a large leak current was observed in APD's after the activation of photocathode. Futhermore larger

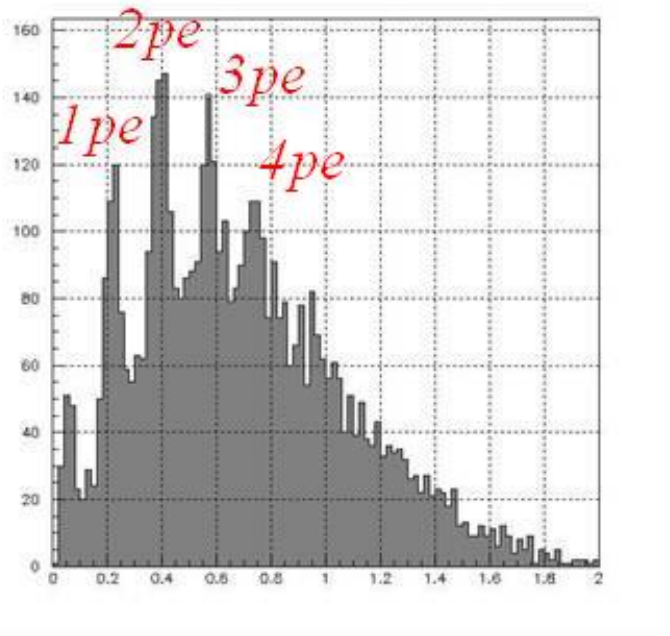

Fig. 23. *Multi-photon spectrum obtained by the single-channel HPD.*

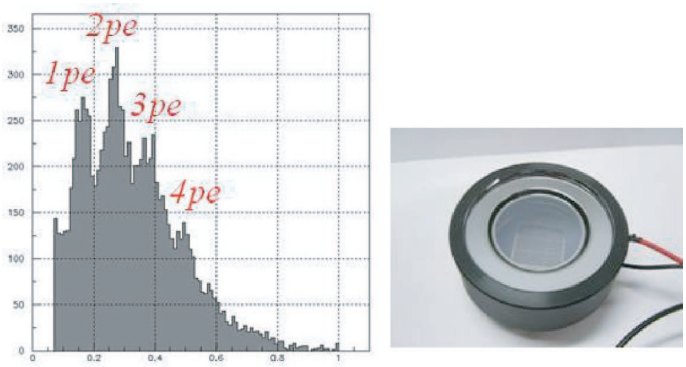

Fig. 24. *Multi-photon spectrum obtained by the 3x3 multi-channel HAPD and a photo of the HAPD.*

noise than expected is seen in APD's. Hamamatsu Photonics is investigating the HAPD's to solve this problem in the next batch. A delivery of prototype 12x12 channel HAPD's is expected in January 2004, and a beam test is planned for February.

References

[1] M.Cantin et al. Nucl. Instr. Meth. **118** (1974) 177.

[2] A.Abashian et al., Nucl. Instr. and Meth. A **479** (2002) 117.

[3] T.Sumiyoshi et al., Nucl. Instr. and Meth. A **433** (1999) 385.

[4] T.Iijima et al., Nucl. Instr. and Meth. A **453** (2000) 321.

[5] I. Adachi et al., Nucl. Instr. and Meth. A **355** (1995) 390390; T. Sumiyoshi et al., J. Non-Cryst. Solids **225** (1998) 369.

[6] D.E.Fields et al. Nucl. Instr. Meth. A **349** (1994) 431.

[7] N.Akopov et al. Nucl. Instr. Meth. A **479**(2002) 511.

[8] T.Ypsilantis and J.Seguinot, Nucl. Instr. Meth. A **368** (1995) 229.

[9] T.Iijima, "Aerogel Cherenkov Counter in Imaging Mode", JPS Meeting, Tokyo Metropolitan University, September 1997.

[10] DEP catalog

[11] I. Adachi et al., "Test of a proximity focusing RICH with aerogel as radiator", Proceedings for the IEEE Nuclear Science Symposium, Norfolk, VA, November 10-15, 2002; hep-ex/0303038; T.Iijima et al., Nucl. Instr. Meth. A **502** (2003) 231.

[12] T. Matsumoto et al., to be published in NIM A; physics/0309032.

[13] H8500 data sheet, Hamamatsu Photonics K.K.

[14] aerogel transmission

[15] Hamamatsu Photonics K.K.

[16] Matsushita Electric Works Ltd. has a Japanese patent (No. 2659155) for usage of DMF as solvent to make aerogel.

[17] A.R. Buzykaev et al. Nucl. Instr. Meth. A **433** (1999) 396.

[18] H.Ikeda et al. Nucl. Instr. Meth. A **372** (1996) 125.

[19] M. Artuso et al., Nucl. Instr. Meth. A **502** (2003) 91.

[20] Ideas SA, Oslo.